



Solid-State Repair of Casting Defects in ZL210 Aluminum Alloy

Zan Lv, Song Han, Wei Hu, Zhibo Dong, Ruofei Huang, and Kang Yang

(Submitted August 17, 2019; in revised form February 8, 2020; published online August 28, 2020)

Casting defects in the ZL210 aluminum alloys were repaired via a solid-state welding method named active-passive filling friction stir repairing (A-PFFSR). Effects of plunge speed on microstructures and mechanical properties of repaired joints were investigated based on a six-spiral-groove pinless tool. Casting defects were firstly machined into a tapered hole by a tapered and threaded pin. Then, the keyhole was successfully repaired by the materials surrounding the keyhole and an extra filler via the A-PFFSR. The lower plunge speed was propitious to improving frictional heat and material flow, which improved joint integrity containing surface appearance and interface joining behaviors. The maximum tensile strength of the repaired joint was approximately equivalent to that of base ZL210 alloys, realizing the quasi-repairing of the ZL210 aluminum alloys.

Keywords casting aluminum alloys, defects repairing, mechanical properties, microstructures, solid-state welding

1. Introduction

Metallic materials have been extensively applied in the manufacturing fields of aerospace, railway and so on, which demand more and more attentions of heat processing techniques (Ref 1-4). When improper process parameters or technological conditions are implemented, the defects are easily formed, which are detrimental to service performances of structural parts (Ref 5-7). Meanwhile, casting aluminum alloys have been widely used in the aerospace and marine manufacturing fields (Ref 8). The casting defects, such as pores, cavities and cracks, deteriorate the service performances of casting structural parts (Ref 9-11).

Although the conventional fusion welding techniques can be used to repair the defects in structural parts, they are restricted due to the pores, coarse grains and cracks induced by extremely high repairing temperature (Ref 12). Recently, a solid-state repairing method based on friction stir welding (FSW) has attracted extensive attentions (Ref 13-16). Aiming at the long volume tunnel and groove defects, Liu and Zhang (Ref 17) put forward the re-FSW method and found that a proper offset could benefit for enhancing joint quality. Ji et al. (Ref 18, 19) proposed vertical compensation friction stir welding (VCFSW) to eliminate groove, tunnel and gap defects, and then obtained a high-quality joint with good surface (Ref 19). For the small

volume defects, such as keyhole, cavity and kissing bond, the main repairing processes can be divided into excavating, filling and welding. Based on FSW, friction taper plug welding (FTPW) (Ref 20), friction bit joining (FBJ) (Ref 21) and filling friction stir welding (FFSW) (Ref 22, 23) have also been proposed, and they all finished the defect repairing by a special-designed consumable filling rotating pin. During FTPW process, a tapered plug contacted with the materials surrounding the defects to be repaired, and then produced frictional heat and plastic flow in a few seconds by forcing the rotating plug (Ref 20). The FBJ process was firstly developed to the spot joining, in which a consumable bit was considered as filler materials. For the FFSW process, a semi-consumable tool containing a consumable filling pin and a no-consumable shoulder was employed to eliminate the keyhole defect, and the tensile strength of the FFSW joint was quasi-equivalent to the excellent FSW joint (Ref 22, 23). For a thin-wall construction, Huang et al. (Ref 24) proposed drilling-filling friction stir repairing (D-FFSR) to repair the keyhole of AZ31 magnesium alloys FSW joints, in which a filling rod material as same as base material (BM) and a pinless tool with the helical structure were used. Moreover, Reimann et al. (Ref 25) employed refill friction stir spot welding (RFSSW) to repair the keyhole of 7075-T651 Al alloys FSW joints, and the tensile strength of the keyhole repairing joint reached 74% of the base strength. The above methods are difficult to repair the volume defect with a big depth. In order to repair volume defects with a depth higher than 3 mm, Ji et al. (Ref 26, 27) proposed active-passive filling friction stir repairing (A-PFFSR) and successfully repaired the 7N01-T4 Al alloys and the AZ31-B Mg alloy, achieving the satisfactory results.

In this study, the microstructure, interface behavior and mechanical properties of the repaired joints via the A-PFFSR characterized by solid-state repairing were mainly investigated in detail, which can provide technical supports for achieving a high-quality joint with uniform microstructures and mechanical properties.

Zan Lv and Song Han have contributed equally to this work.

Zan Lv, Song Han, Wei Hu, Ruofei Huang, and Kang Yang, College of Aerospace Engineering, Shenyang Aerospace University, Shenyang 110136, China; and **Zhibo Dong**, State Key Laboratory of Advanced Welding and Joining, Harbin Institute of Technology, Harbin 150001, China. Contact e-mails: huwei201805@126.com and dongzhibo@hit.edu.cn.

2. Experimental Procedures

The BM was ZL210 aluminum alloy with a T5 temper in this experiment, whose dimension was $200 \times 100 \times 6 \text{ mm}^3$. The casting defects are shown in Fig. 1. A series of tools containing the six-spiral-flute shoulder were employed, which were beneficial to improving the material flow and then enhancing the solid-state bonding. Schematic of the A-PFFSR is exhibited in Fig. 2. Before the repairing process, the casting

defects were firstly machined into a tapered hole by a tool with a threaded pin. The A-PFFSR process was divided into active filling (AF) and passive filling (PF) stages. During the AF stage, the rotating tool without pin plunges into the taper hole and then returns. The materials surrounding the keyhole were continuously squeezed into the keyhole by a pinless tool and then filling the keyhole to a certain depth. For the PF stage, an extra filler was put into the enlarged keyhole with a relatively small depth produced by the AF stage, and then, the filler was softened and transferred under the high temperature and

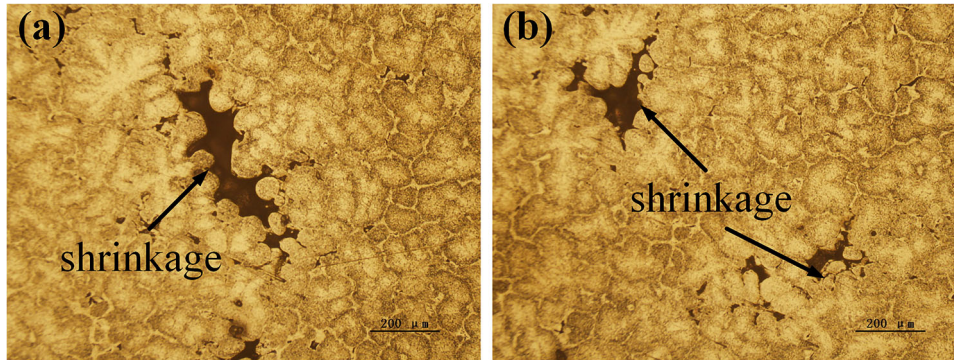


Fig. 1 Casting defects in the ZL210 alloy

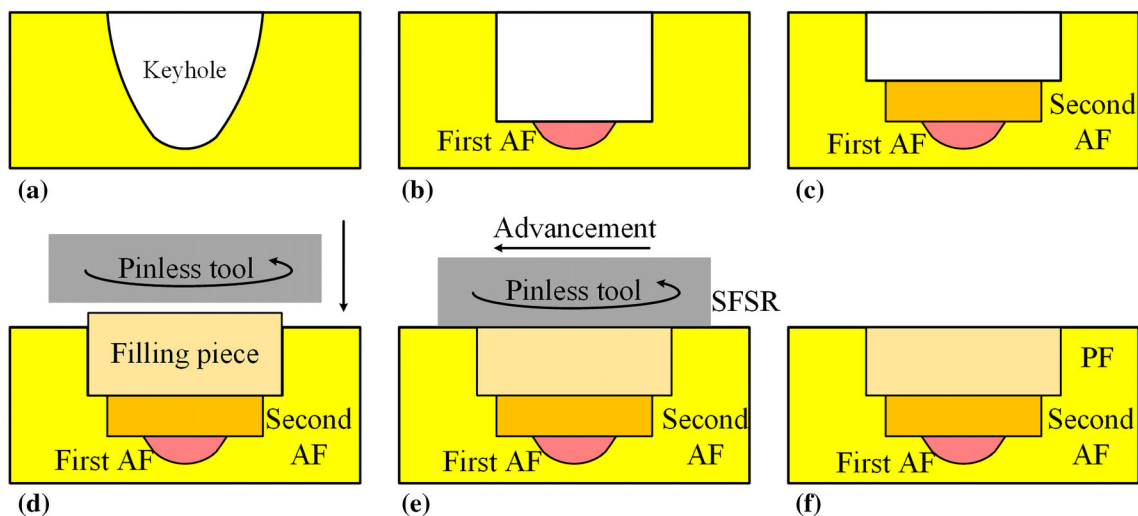


Fig. 2 Schematics of the A-PFFSR: (a) keyhole, (b) first active filling, (c) second active filling, (d) addition of filling piece, (e) SFSR and (f) completion of A-PFFSR

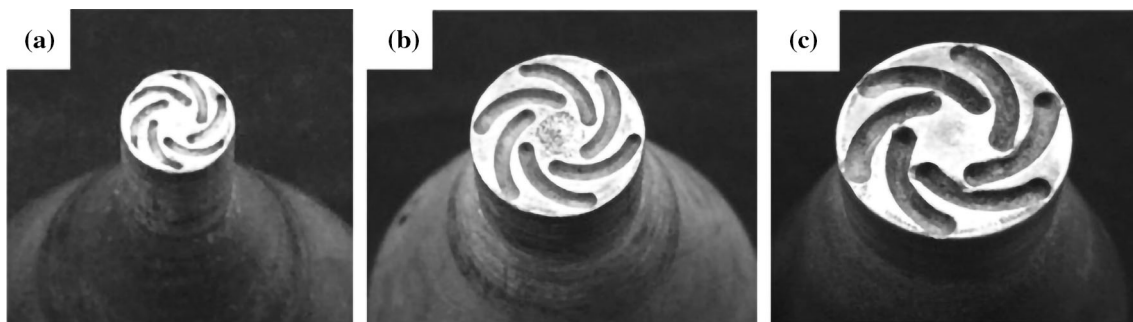


Fig. 3 Pinless tools with different shoulder diameters in the repairing process: (a) 6 mm, (b) 10 mm and (c) 14 mm

material flow produced by the rotation of the pinless tool. Finally, a surface friction stir repairing (SFSR) stage was performed, which was the rotational tool moved straightly for 15 mm after dwelling for 5 s. Consequently, the volume defects, such as the keyhole, could be completely repaired. In this study, the keyhole was produced by the tool with a 4 mm pin, so the two AF stages which were named, respectively, first AF and second AF stages were used. The shoulder diameters for the first and second AF stages were, respectively, 6 mm and 10 mm, and the corresponding repairing depths were 1 mm and 1.5 mm. Meanwhile, the shoulder with a 14 mm diameter was used during the PF stage and its repairing depth was 1.5 mm. The repairing pinless tools used in this study are shown in Fig. 3, and these pinless tools rotated clockwise (Ref 26). The height of the extra filler used in the PF stage was 2 mm. The rotating velocity was 1600 rpm. A tilting angle relative to the Z-axis was 2.5°. The investigated plunge speeds were 1, 2, 4 and 6 mm/min, respectively.

In order to better analyze thermal cycle of filling zone (FZ) during the A-PFFSR process, the K-type thermocouples were used to measure temperature profile. The schematic diagram of the K-type thermocouples locations is shown in Fig. 4. Although the distance from the measured point to the center of the repairing zone is 9.5 mm, the temperature variation trend of measured point can reflect that of FZ. This is because the heat is conducted from FZ to the thermocouples location. A digital data logger was applied to record the temperature history of each location at a frequency of 1 Hz.

The metallurgical specimens were cut from the repaired joints. After polished firstly by different grades of emery papers and then by the disk polishing machine, the metallurgical specimen was observed using an optical microscope (OM). Three flat dogbone-shaped specimens were cut by an electrical discharge machine to evaluate the tensile properties. At room temperature which was 25 °C, the tensile tests were carried out at a constant crosshead speed of 1 mm/min. Fracture surface

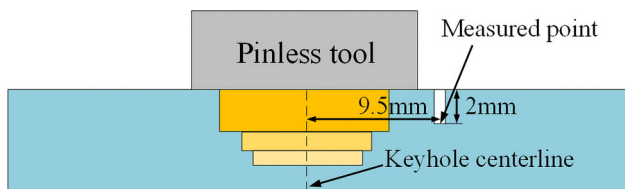


Fig. 4 Schematic of thermocouple locations during temperature measurement

morphologies of the repaired joint were characterized by a scanning electron microscope (SEM). Microhardness of the repaired joint was measured by a microhardness tester at a load of 200 g for 10 s, while the interval between adjacent two points was 0.5 mm.

3. Results and Discussion

3.1 Joint Formation

Table 1 shows the surface morphologies of the repaired joints by different plunge speeds. In order to analyze the influence of plunge speed on surface formation, the temperatures during the repairing processes were measured, and the temperature profiles are indicated in Fig. 5. From Fig. 5, it is known that with the increase in plunge speed, the peak temperature in the FZ is decreased, and then, the insufficient material flow is obtained (Ref 28). When the plunge speed is 1 mm/min, the surface appearance is relatively smooth and few flashes are formed. This is because the low plunge speed can preheat the repaired materials for long time and then improve the material transfer behaviors, achieving the satisfactory surface integrity. With increasing plunge speed to 2 mm/min, the joint surface appearance similar to that of 1 mm/min is

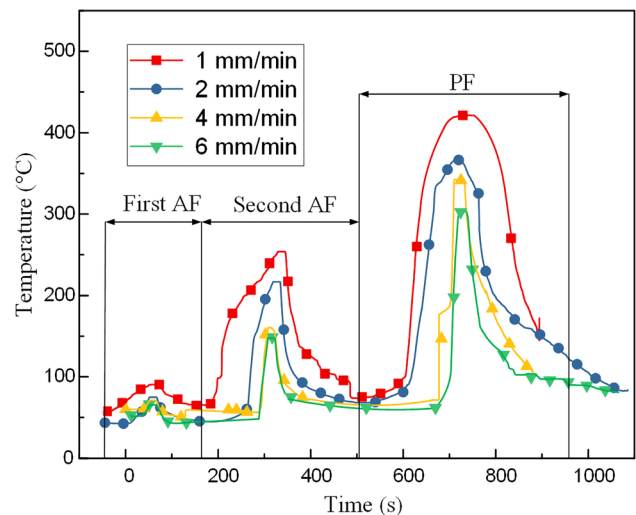


Fig. 5 Temperature profiles of repaired processes by different plunge speeds

Table 1 Surface appearances of the repaired joints by different plunge speeds

1 mm/min	2mm/min	4mm/min	6mm/min

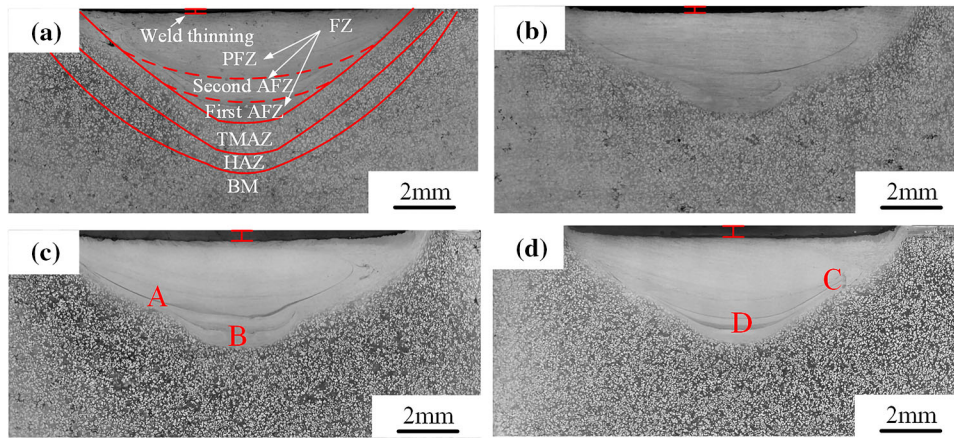


Fig. 6 Macrostructures of repaired joints by different plunge speeds: (a) 1 mm/min, (b) 2 mm/min, (c) 4 mm/min and (d) 6 mm/min

attained due to the sufficient frictional heat and material flow. However, when the plunge speed is 4 mm/min, the frictional heat is significantly decreased. The insufficient heat input resulting from higher plunge speed is difficult to reduce the flow stress and increase material flow, which causes that the plasticized materials are difficult to be transferred from the edge to the center of shoulder, producing the wave shape morphology.

Compared with 4 mm/min, the bigger flashes appear at 6 mm/min due to the lower temperature. The extremely reduced heat input is hard to soften the repaired materials, and then, these materials are difficult to be transferred and exert a lower counterforce on the pinless tool, producing the big flashes. It can be concluded that a relatively lower plunge speed produces more heat input and is suitable to the surface integrity of the repaired joint.

3.2 Microstructures and Interfacial Behaviors

Figure 6 displays the macrostructures in cross sections of repaired joints by different plunge speeds. The interfacial characteristics between the repairing interfaces directly determine the repaired quality (Ref 29). The A-PFFSR joint is divided into four typical zones, namely BM, thermo-mechanically affected zone (TMAZ), heat-affected zone (HAZ) and FZ. The FZ consists of active filling zone (AFZ) and passive filling zone (PFZ). Moreover, the AFZ includes first active filling zone (first AFZ) and second active filling zone (second AFZ).

As listed in Table 2, there are no defects appear at the TMAZ and the PFZ of the joints by the plunge speeds of 1 mm/min and 2 mm/min, indicating the good metallurgical bonding, which results from the sufficient solid-state diffusion due to the relatively higher frictional heat (Fig. 5) and sufficient material flow. Moreover, lower weld thinning is formed at the surface of the repaired joint by the lower plunge speeds (Fig. 6a and b). As exhibited in Fig. 7, the defects are formed at the joining interfaces, which results from that the insufficient frictional heat and material flow induced by higher plunge speed. The defect

becomes the stress concentration source during the tensile test, and then deteriorates the mechanical properties.

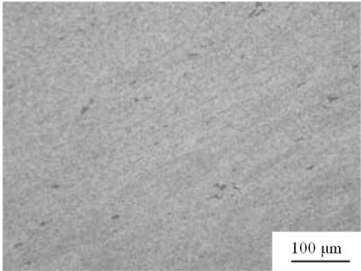
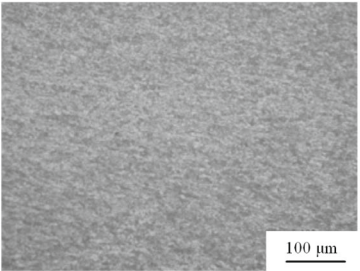
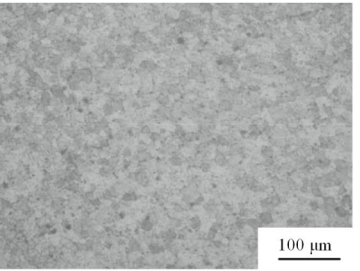
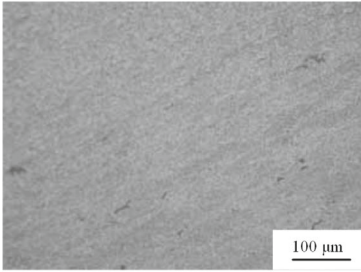
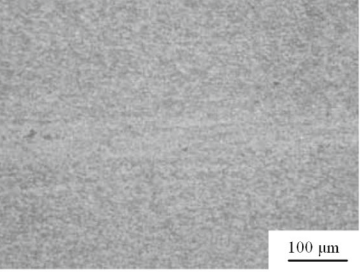
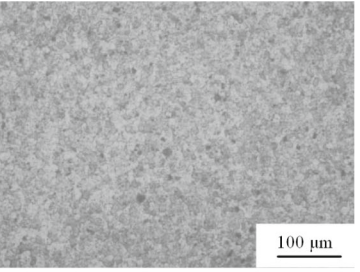
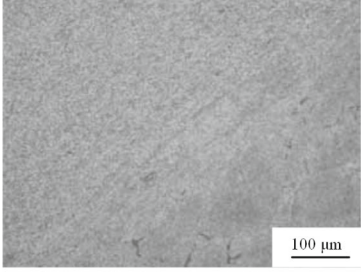
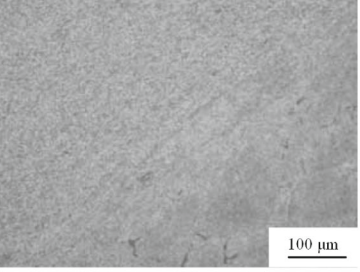
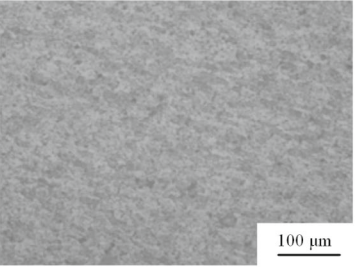
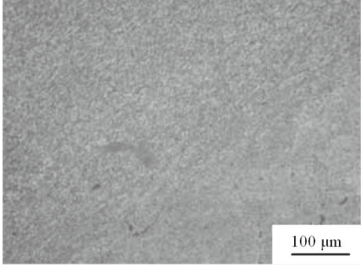
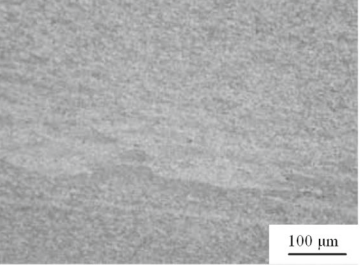
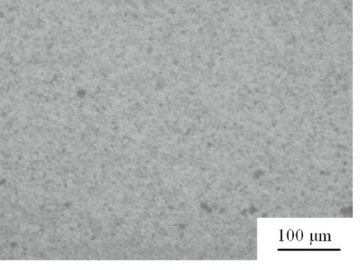
3.3 Microhardness

Figure 8 exhibits the microhardness distribution of the repaired joints by different plunge speeds. The microhardness distribution presents a “W” shape, while the higher values are formed in the FZ and the lower values appear in the HAZ. The welding thermal cycle exerts significant role on the dissolution, re-precipitation and coarsening of strengthening precipitates (Ref 2, 30-32), consequently reducing the microhardness. Meanwhile, according to the Hall-Petch relation (Ref 29), the finer the grain size, the higher the microhardness. In this study, the dynamic recrystallization in the FZ leads to the finer and equiaxed grains, which effectively improves the microhardness values to a certain extent. The materials in the HAZ suffer from high heat input, resulting in the grain coarsening and further decreasing the hardness value. Meanwhile, the microhardness values of the first AFZ are higher (90 HV), which is because the materials in the first AFZ contact with the backing plate and then facilitate the heat transfer and dissipation. For the materials in the second AFZ, the heat input is difficult to dissipate, further resulting in the decrease in the microhardness (83 HV). The materials in the PFZ are directly exposed in the atmosphere, and the heat convection can slightly decrease the total heat input in the weld, resulting in the slightly higher values (87 HV) compared with the second AFZ. Moreover, the microhardness values in the FZ at the plunge speed of 2 mm/min are slightly lower than those of joints at the plunge speed of 6 mm/min. Awang et al. (Ref 33) stated that a high plunge speed produced lower frictional heat per unit time, which effectively inhibited the grain growth. It can be concluded that the plunge speed has no obvious effect on microhardness values.

3.4 Tensile Properties

Figure 9 and 10 displays tensile results of the repaired joints at different plunge speeds. With the increase in the plunge

Table 2 Interfacial microstructures of the repaired joints by different plunge speeds

ω	TMAZ	Interface between PFZ and second AFZ	PFZ
1 mm/min			
2 mm/min			
4 mm/min			
6 mm/min			

speed, the tensile strengths of the repaired joints gradually decrease due to the weld thinning and interfacial defects. At the plunge speed of 1 mm/min, the maximum tensile strength of the repaired joint is quasi-equivalent to BM due to the reduction of weld thinning and elimination of interfacial defects induced by the improved frictional heat (Fig. 5) and material flow, and the tensile fracture does not locate at the FZ (Fig. 10b). For the relatively higher plunge speed, the insufficient frictional heat and material flow result in the interfacial defects (Fig. 7) and the weld thinning (Fig. 6c and d). These two phenomena,

respectively, produce the stress concentration and reduce the bearing area of the repaired joint, which greatly decreases the tensile properties and leads to the fracture located at the FZ (Fig. 10a).

Figure 11 shows the fracture surface morphologies which are obtained with an SEM of the repaired joints owning the lower and higher tensile strengths. For the repaired joint with higher tensile strength at the plunge speed of 1 mm/min, various dimples are observed on the fracture surface, as exhibited in Fig. 11(a) and (b). This indicates the typical ductile

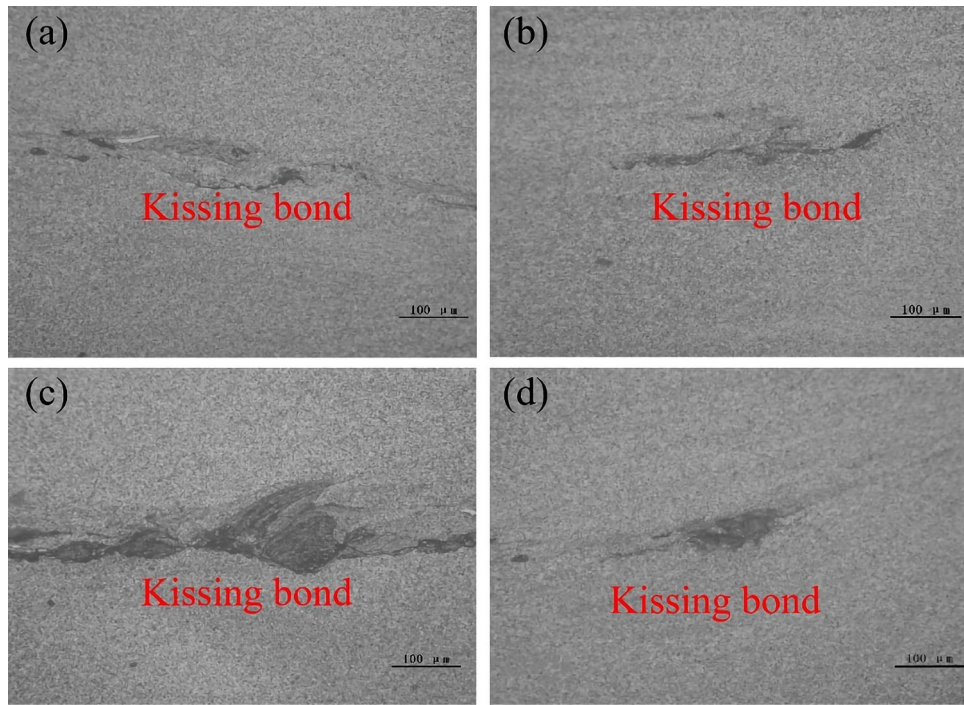


Fig. 7 Interfacial defects in the repaired joints: (a) and (b) A and B marked in Fig. 6(c), (c) and (d) C and D marked in Fig. 6(d)

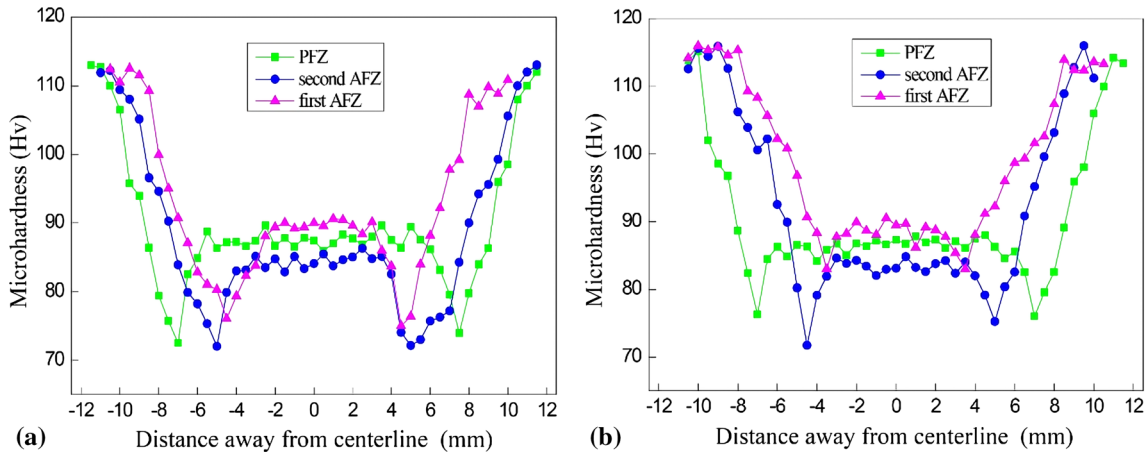


Fig. 8 Microhardness distributions of the repaired joints with different plunge speeds: (a) 2 mm/min and (b) 6 mm/min

fracture, which corresponds to the fracture location in the BM. For the repaired joint with the lower tensile strength at the plunge speed of 6 mm/min, some cleavage morphologies (Fig. 11c) are presented on the fracture surfaces, which results from the interfacial defect in the FZ. Meanwhile, few dimples appear on the fracture surface locating at the repairing interfaces, as shown in Fig. 11(d), which indicates the good

interfacial joining is still formed at the repairing interfaces. From the macrostructures, microstructures and mechanical properties mentioned above, it can be concluded that the lower plunge speed is beneficial to eliminating the interfacial defects and then improving the tensile strength of the repaired joint for cast aluminum alloy.

4. Conclusions

Cast defects in the ZL210 aluminum alloys were successfully eliminated by the A-PFFSR, which effectively avoided the shrinkages, pores and cavities defects accompanied with the fusion welding process.

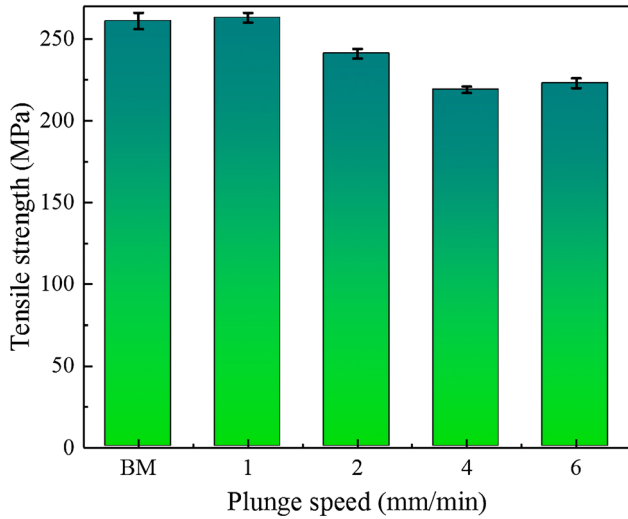


Fig. 9 Tensile strengths of the BM and repaired joints by different plunge speeds

1. Joint formation: Owing to the differences in heat input and material flow, the surface appearance was relatively smooth at the lower plunge speed, while the wave shape morphology with big flashes appeared at higher plunge speed.
2. Microstructures and interface behavior: With increasing the plunge speed, the interfacial defects and the welding thinning easily appeared, which were harmful to tensile strength of the repaired joint.
3. Mechanical properties: The repaired joint with the highest tensile strength quasi-equivalent to that of BM was obtained at the plunge speed of 1 mm/min. The fracture surface morphologies of the sound joint presented the typical ductile fracture characterized by dimples with varied sizes.

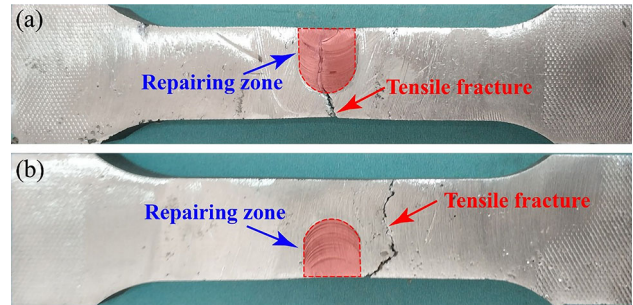


Fig. 10 Fracture locations of the repaired joints by different plunge speeds: (a) 1 mm/min and (b) 6 mm/min

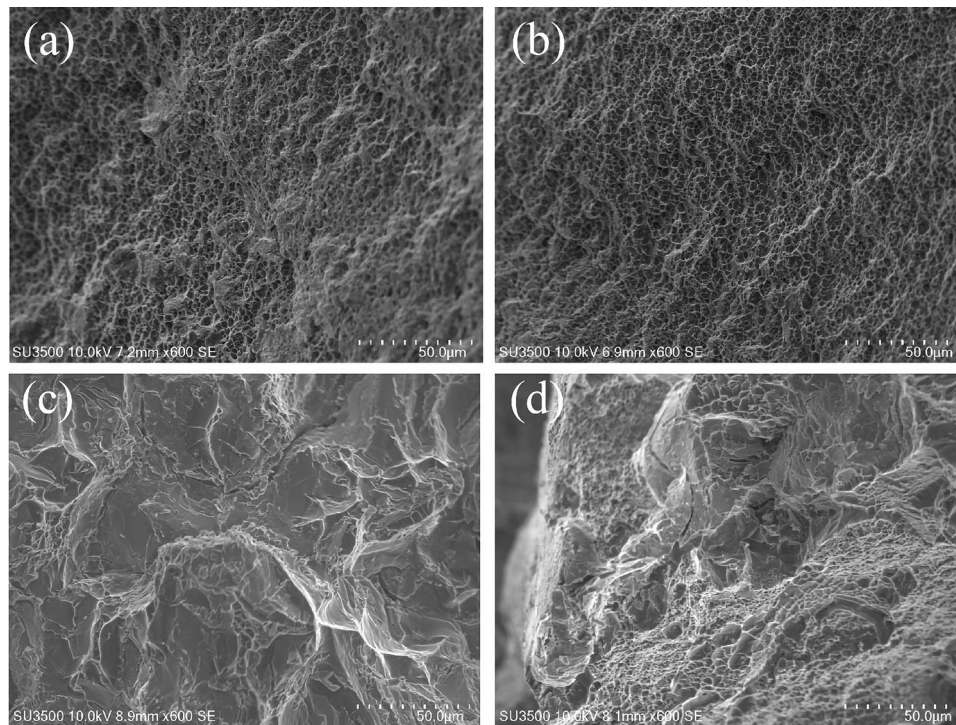


Fig. 11 Fracture surface morphologies of the repaired joints at different plunge speeds: (a) and (b) 1 mm/min, (c) and (d) 6 mm/min

Acknowledgment

This work is supported by the National Natural Science Foundation of China (No. 51874201) and the Education Department Foundation of Liaoning Province (No. L201740).

References

1. H.J. Liu, J.Q. Li, and W.J. Duan, Friction Stir Welding Characteristics of 2219-T6 Aluminum Alloy Assisted by External Non-Rotational Shoulder, *Int. J. Adv. Manuf. Technol.*, 2013, **64**(9–12), p 1685–1694
2. Y. Chen, H. Liu, and J. Feng, Friction Stir Welding Characteristics of Different Heat-Treated-State 2219 Aluminum Alloy Plates, *Mater. Sci. Eng., A*, 2006, **420**(1–2), p 21–25
3. L. Zhou, K. Nakata, J. Liao, and T. Tsumura, Microstructural Characteristics and Mechanical Properties of Non-Combustive Mg-9Al-Zn-Ca Magnesium Alloy Friction Stir Welded Joints, *Mater. Des.*, 2012, **42**, p 505–512. <http://doi.org/10.1016/j.matdes.2012.06.005>
4. K. Gangwar and M. Ramulu, Friction Stir Welding of Titanium Alloys: A Review, *Mater. Des.*, 2018, **141**, p 230–255. <http://doi.org/10.1016/j.matdes.2017.12.033>
5. X.H. Zeng, P. Xue, D. Wang, D.R. Ni, B.L. Xiao, and Z.Y. Ma, Effect of Processing Parameters on Plastic Flow and Defect Formation in Friction-Stir-Welded Aluminum Alloy, *Metall. Mater. Trans. A Phys. Metall. Mater. Sci.*, 2018, **49**(7), p 2673–2683
6. Y. Lv, Y. Ding, Y. Han, L. Wu, L. Wang, and W. Lu, Effect of Microstructures on Fatigue Crack Growth Behavior of Friction Stir Processed NiAl Bronze Alloy, *Metall. Mater. Trans. A Phys. Metall. Mater. Sci.*, 2017, **48**(3), p 1121–1132
7. W. Li, J. Li, Z. Zhang, D. Gao, W. Wang, and C. Dong, Improving Mechanical Properties of Pinless Friction Stir Spot Welded Joints by Eliminating Hook Defect, *Mater. Des.*, 2014, **62**, p 247–254. <http://doi.org/10.1016/j.matdes.2014.05.028>
8. S. Ji, R. Huang, L. Zhang, X. Meng, and Z. Lv, Microstructure and Mechanical Properties of Friction Stir Repaired Al–Cu Casting Alloy, *Trans. Indian Inst. Met.*, 2018, **71**(8), p 2057–2065. <http://doi.org/10.1007/s12666-018-1340-x>
9. B. Han, W.J. Wan, C.L. Zhu, J. Zhang, and J.H. Yi, Effect of Casting Defects on High Cycle Fatigue Life of Fully Lamellar TiAl Alloy, *Mater. Res. Innov.*, 2015, **19**(sup4), p S142–S146
10. L. Lattanzi, A. Fabrizi, A. Fortini, M. Merlin, and G. Timelli, Effects of Microstructure and Casting Defects on the Fatigue Behavior of the High-Pressure Die-Cast AlSi9Cu3(Fe) Alloy, *Procedia Struct. Integr.*, 2017, **7**, p 505–512
11. D.F. Susan, T.B. Crenshaw, and J.S. Gearhart, The Effects of Casting Porosity on the Tensile Behavior of Investment Cast 17-4PH Stainless Steel, *J. Mater. Eng. Perform.*, 2015, **24**(8), p 1–2
12. L. Li, Z. Liu, and M. Snow, Effect of Defects on Fatigue Strength of GTAW Repaired Cast Aluminum Alloy, *Weld. J.*, 2006, **85**(11), p 264s–270s
13. I. Kalembarac, C. Hamilton, M. Kopycianski, D. Miara, and K. Krasnowski, Microstructure and Mechanical Properties of Friction Stir Welded 5083 and 7075 Aluminum Alloys, *J. Mater. Eng. Perform.*, 2017, **26**(3), p 1–12
14. S. Ji and Z. Li, Reducing the Hook Defect of Friction Stir Lap Welded Ti-6Al-4V Alloy by Slightly Penetrating into the Lower Sheet, *J. Mater. Eng. Perform.*, 2017, **26**(2), p 1–10
15. L. Esposito, A. Bertocco, G. Cricri, and V. Rosiello, Welding-Repair Effect on F357-T6 Aluminum Castings: Analysis of Fatigue Life, *Int. J. Adv. Manuf. Technol.*, 2019, **102**(9–12), p 3699–3706
16. L. Ma, S. Niu, S. Ji, and P. Gong, Comparative Study of 2060-T8 Al-Li Alloy Friction Stir Welded Joints between Natural Cooling and Water Cooling, *Arch. Metall. Mater.*, 2020, **65**(1), p 307–314
17. H. Liu and H. Zhang, Repair Welding Process of Friction Stir Welding Groove Defect, *Trans. Nonferr. Met. Soc. China*, 2009, **19**(3), p 563–567. [http://doi.org/10.1016/S1003-6326\(08\)60313-1](http://doi.org/10.1016/S1003-6326(08)60313-1)
18. S. Ji, X. Meng, J. Xing, L. Ma, and S. Gao, Vertical Compensation Friction Stir Welding of 6061-T6 Aluminum Alloy, *High Temp. Mater. Process.*, 2016, **35**(8), p 843–851. <http://doi.org/10.1515/htmp-2015-0063>
19. S. Ji, X. Meng, L. Ma, H. Lu, and S. Gao, Vertical Compensation Friction Stir Welding Assisted by External Stationary Shoulder, *Mater. Des.*, 2015, **68**, p 72–79. <http://doi.org/10.1016/j.matdes.2014.12.009>
20. J. Xiong, X. Yang, W. Lin, and K. Liu, Evaluation of Inhomogeneity in Tensile Strength and Fracture Toughness of Underwater Wet Friction Taper Plug Welded Joints for Low-Alloy Pipeline Steels, *J. Manuf. Process.*, 2018, **32**, p 280–287. <http://doi.org/10.1016/j.jmapro.2018.02.016>
21. Y.C. Lim, L. Squires, T.Y. Pan, M. Miles, G.L. Song, Y. Wang, and Z. Feng, Study of Mechanical Joint Strength of Aluminum Alloy 7075-T6 and Dual Phase Steel 980 Welded by Friction Bit Joining and Weld-Bonding under Corrosion Medium, *Mater. Des.*, 2015, **69**, p 37–43. <http://doi.org/10.1016/j.matdes.2014.12.043>
22. Y.X. Huang, B. Han, Y. Tian, H.J. Liu, S.X. Lv, J.C. Feng, J.S. Leng, and Y. Li, New Technique of Filling Friction Stir Welding, *Sci. Technol. Weld. Join.*, 2011, **16**(6), p 497–501. <http://doi.org/10.1179/1362171811Y.0000000032>
23. B. Han, Y. Huang, S. Lv, L. Wan, J. Feng, and G. Fu, AA7075 Bit for Repairing AA2219 Keyhole by Filling Friction Stir Welding, *Mater. Des.*, 2013, **51**, p 25–33. <http://doi.org/10.1016/j.matdes.2013.03.089>
24. R. Huang, S. Ji, X. Meng, and Z. Li, Drilling-Filling Friction Stir Repairing of AZ31B Magnesium Alloy, *J. Mater. Process. Technol.*, 2018, **255**, p 765–772. <http://doi.org/10.1016/j.jmatprotec.2018.01.019>
25. M. Reimann, J. Goebel, and J.F. dos Santos, Microstructure and Mechanical Properties of Keyhole Repair Welds in AA 7075-T651 Using Refill Friction Stir Spot Welding, *Mater. Des.*, 2017, **132**, p 283–294. <http://doi.org/10.1016/j.matdes.2017.07.013>
26. S. Ji, X. Meng, Y. Zeng, L. Ma, and S. Gao, New Technique for Eliminating Keyhole by Active-Passive Filling Friction Stir Repairing, *Mater. Des.*, 2016, **97**, p 175–182. <http://doi.org/10.1016/j.matdes.2016.02.088>
27. S.D. Ji, X.C. Meng, R.F. Huang, L. Ma, and S.S. Gao, Microstructures and Mechanical Properties of 7N01-T4 Aluminum Alloy Joints by Active-Passive Filling Friction Stir Repairing, *Mater. Sci. Eng., A*, 2016, **664**, p 94–102
28. R. Padmanaban, V.R. Kishore, and V. Balusamy, Numerical Simulation of Temperature Distribution and Material Flow During Friction Stir Welding of Dissimilar Aluminum Alloys, *Procedia Eng.*, 2014, **97**, p 854–863
29. S. Niu, B. Wu, L. Ma, Z. Lv, and D. Yan, Passive Filling Friction Stir Repairing AZ31-B Magnesium Alloy by External Stationary Shoulder, *Int. J. Adv. Manuf. Technol.*, 2018, **97**(5–8), p 2461–2468. <http://doi.org/10.1007/s00170-018-2130-7>
30. H.J. Liu, H. Fujii, M. Maeda, and K. Nogi, Tensile Properties and Fracture Locations of Friction-Stir-Welded Joints of 2017-T351 Aluminum Alloy, *J. Mater. Process. Technol.*, 2003, **142**(3), p 692–696
31. S.D. Ji, X.C. Meng, Z.W. Li, L. Ma, and S.S. Gao, Investigation of Vertical Compensation Friction Stir-Welded 7N01-T4 Aluminum Alloy, *Int. J. Adv. Manuf. Technol.*, 2016, **84**(9–12), p 2391–2399
32. W.F. Xu, X.K. Wu, J. Ma, H.J. Lu, and Y.X. Luo, Abnormal Fracture of 7085 High Strength Aluminum Alloy Thick Plate Joint via Friction Stir Welding, *J. Mater. Res. Technol.*, 2019, **8**(6), p 6029–6040. <http://doi.org/10.1016/j.jmrt.2019.09.077>
33. M. Awang and V.H. Mucino, Energy Generation during Friction Stir Spot Welding (FSSW) of Al 6061-T6 Plates, *Mater. Manuf. Process.*, 2010, **25**(1–3), p 167–174

Publisher's Note Springer Nature remains neutral with regard to jurisdictional claims in published maps and institutional affiliations.